

Coexistence of Spin Density Wave and Metallic Phases Under Pressure

**A. L. Rakhmanov, K. I. Kugel &
A. O. Sboychakov**

**Journal of Superconductivity and
Novel Magnetism**

ISSN 1557-1939
Volume 33
Number 8

J Supercond Nov Magn (2020)
33:2405-2413
DOI 10.1007/s10948-019-05379-z

Your article is protected by copyright and all rights are held exclusively by Springer Science+Business Media, LLC, part of Springer Nature. This e-offprint is for personal use only and shall not be self-archived in electronic repositories. If you wish to self-archive your article, please use the accepted manuscript version for posting on your own website. You may further deposit the accepted manuscript version in any repository, provided it is only made publicly available 12 months after official publication or later and provided acknowledgement is given to the original source of publication and a link is inserted to the published article on Springer's website. The link must be accompanied by the following text: "The final publication is available at link.springer.com".



Coexistence of Spin Density Wave and Metallic Phases Under Pressure

A. L. Rakhmanov^{1,2,3} · K. I. Kugel^{1,4} · A. O. Sboychakov¹

Received: 17 November 2019 / Accepted: 29 November 2019 / Published online: 29 January 2020
© Springer Science+Business Media, LLC, part of Springer Nature 2020

Abstract

Using a simple and rather general model of the system with imperfect nesting of the Fermi surface, we show that the spin density wave (SDW) and normal metal (or, at low temperature, a superconductor) can coexist within a certain pressure range due to the electronic phase separation. The model predicts the SDW state at low pressure, then, the nucleation of paramagnetic (PM) droplets or islands within the SDW host at higher pressure. When the pressure continues to increase, the droplets transform to rods (or pillars) and, finally, to slabs. With the further growth of pressure, a uniform metallic phase arises. The theory agrees well with the experiment and, even in its simplest version, can capture the essential physics of the systems under study.

Keywords Electronic phase separation · Imperfect nesting · Spin density wave

1 Introduction

The coexistence of antiferromagnetic (AFM) and metallic (often superconducting at low temperatures) phases is one of the most intriguing problem in strongly correlated materials. The interplay of these orders is observed in a number of important systems, e.g., in the superconducting cuprates, pnictides, heavy fermion superconductors, and organic metals. There is no consensus concerning the mechanisms giving rise to such coexistence; it is not clear

whether we are dealing with a uniform state or inhomogeneous one. If inhomogeneous, is this inhomogeneity due to the phase separation, soliton domain walls, or to something else? However, the experiments [1–4] with an archetypical Bechgaard salt (TMTSF)₂PF₆ under high pressure shed light on the problem, at any rate for these specific systems. In Ref. [1], we find clear indications to the coexistence of the spin density wave (SDW) and paramagnetic (PM) metallic phases manifesting itself in the form of phase separation with macroscopic domains of the high-pressure PM metallic phase embedded into the insulating SDW host, which are aligned along certain crystallographic axes.

Let us mention here that these pressure effects have certain similarity with the situation in transition metal oxides, where the strain in the lattice is tuned by internal pressure [5, 6] or by the electron–lattice interaction [7]. This tuning gives rise to a quite rich picture of the phase separation occurring owing to the interplay of spin, charge, and elastic (related to the internal pressure) degrees of freedom are also actively discussed in the case of nickelates [9–11]. Note in addition that the pressure effect on the phase separation should be especially clearly pronounced in the vicinity of the Lifshitz transition, where the Fermi surface topology undergoes certain changes [12–14].

In this paper, we incorporate the effect of pressure in a classical Rice model [15, 16] for the systems with

✉ K. I. Kugel
klimkugel@gmail.com

A. L. Rakhmanov
alrakhmanov@mail.ru

A. O. Sboychakov
sboycha@mail.ru

¹ Institute for Theoretical and Applied Electrodynamics, Russian Academy of Sciences, Moscow 125412, Russia

² Dukhov Research Institute of Automatics, Moscow 127055, Russia

³ Moscow Institute for Physics and Technology (National Research University), Dolgoprudny, Moscow Region 141700, Russia

⁴ National Research University Higher School of Economics, Moscow 101000, Russia

imperfect nesting in the framework of the simplest possible scheme. Similar models are used to describe the electronic properties of superconducting iron pnictides and iron chalcogenides [17–21], AA-stacked graphene bilayers [22], and other systems [23]. In our earlier papers [24, 25], we have shown that this model predicts a phase separation within certain ranges of doping, temperature, and magnetic field. Here, we demonstrate that the application of pressure also gives rise to the phase separation, that is, to the transformation of the uniform SDW state to a mixture of SDW and PM metallic regions. The cause of such effect is the same as in the case of doping or magnetic field: the pressure shifts the system from the position of a perfect nesting. Note that the nesting of the Fermi surface is a common feature of the Bechgaard salts [1].

The phase separation violates the charge neutrality of the system. We take into account the electrostatic energy of the inhomogeneous state and the energy of interfaces between SDW and PM metal following the approach proposed in Refs. [26] and [27]. As a result, we are able to trace the evolution of the system with the increase in pressure from the uniform SDW state to the phase-separated state (PS) with PM metallic islands (or droplets) in the SDW matrix, which become transformed into pillars (or rods), then, into slabs, and, finally, into the uniform PM metallic state. Naturally, the PM metal may be superconducting at low temperatures. It is of importance that even such a simple and rather general approach allows us to describe the experimental results reported in Ref. [1].

The paper is organized as follows. For the readers' convenience, in Section 2, we present a detailed description of the model for the system with imperfect nesting and show how the effect of pressure could be incorporated into this model. In Section 3, we calculate the phase diagram of the system in the pressure–temperature plane. In Section 4, we take into account the long-range Coulomb interaction and the interface energy between different phases to reproduce the evolution of the geometry of the inhomogeneous phase with pressure. In Section 5, we briefly analyze the obtained results and compare them with the experiment in Ref. [1].

2 Model

We apply the model proposed by Rice [15] to describe the AFM state in chromium. The band structure corresponding to the model includes one spherical electron pocket, one spherical hole pocket, and additional band or bands, which do not participate in the magnetic ordering (reservoir). To describe the SDW, we can ignore all interactions except the repulsion between electrons in the pockets involved to

the ordering. The system is a three-dimensional one and its Hamiltonian has the form:

$$\hat{H} = \sum_{\mathbf{k}\sigma\alpha} \epsilon^\alpha(\mathbf{k}) n_{\mathbf{k}\sigma}^\alpha + \frac{V}{\mathcal{V}} \sum_{\substack{\mathbf{k}\mathbf{k}'\mathbf{q} \\ \sigma\sigma'}} a_{\mathbf{k}+\mathbf{q}\sigma}^\dagger a_{\mathbf{k}\sigma} b_{\mathbf{k}'-\mathbf{q}\sigma'}^\dagger b_{\mathbf{k}'\sigma'}, \quad (1)$$

where α is equal to either a (electron pocket), b (hole pocket), or c (nonmagnetic bands), $a_{\mathbf{k}\sigma}^\dagger$ ($b_{\mathbf{k}\sigma}^\dagger$) is the creation operator of the electron (hole) with momentum \mathbf{k} and spin projection σ , n^α is the electron or hole number operator, V is the Coulomb interaction, and \mathcal{V} is the volume. The nonmagnetic noninteracting band c has the density of states N_r at the Fermi energy. We assume a quadratic dispersion law for both pockets and use the Wigner–Seitz approximation. In the electron pocket, the wave vector \mathbf{k} is located within a sphere of finite radius centered at zero momentum. In the hole pocket, such sphere is centered at \mathbf{Q}_0 . The energies $\epsilon^\alpha(\mathbf{k})$ of these states lie between the minimum values ($\epsilon_{\min}^{a,b}$) and maximum values ($\epsilon_{\max}^{a,b}$). The energy spectra for the electron and hole pockets, measured relative to the Fermi energy μ , can be expressed as ($\hbar = 1$):

$$\begin{aligned} \epsilon^a(\mathbf{k}) &= \frac{\mathbf{k}^2}{2m_a} + \epsilon_{\min}^a - \mu, \\ \epsilon^b(\mathbf{k} + \mathbf{Q}_0) &= -\frac{\mathbf{k}^2}{2m_b} + \epsilon_{\max}^b - \mu. \end{aligned} \quad (2)$$

The perfect nesting means that the Fermi surfaces of the a and b pockets coincide at some $\mu = \mu_0$ and both Fermi spheres have the same Fermi momentum $k_{Fa} = k_{Fb} = k_F$. From (2), we get:

$$\mu_0 = \frac{m_a \epsilon_{\min}^a + m_b \epsilon_{\max}^b}{m_a + m_b}, \quad k_F^2 = \frac{2m_a m_b}{m_a + m_b} (\epsilon_{\max}^b - \epsilon_{\min}^a). \quad (3)$$

For example, in the case of perfect electron–hole symmetry, when $m_a = m_b = m$ and $\epsilon_{\max}^b = -\epsilon_{\min}^a = \epsilon_F$, we obtain $\mu_0 = 0$. Below, we assume that $\mu_0 = 0$, or, in other words, we will measure the chemical potential from its value at the perfect nesting. In what follows, we are interested in the case when the system is not far from the perfect nesting, that is $|\mu| \ll \epsilon_F$. Then, expanding the spectra (2) near the Fermi momentum k_F , we obtain:

$$\epsilon^a \approx v_F \delta k - \mu, \quad \epsilon^b \approx -v_F \delta k - \mu, \quad (4)$$

where $v_F = k_F/m$ and $\delta k = |\mathbf{k}| - k_F$.

In Hamiltonian (1), we assume a weak-coupling regime, that is, $V N_F \ll 1$, where $N_F = k_F^3/2\pi^2 \epsilon_F$. We treat Hamiltonian (1) using a BCS-like mean-field approximation since it is an asymptotically exact approach in the limit

$V N_F \rightarrow 0$. Following Refs. [15, 24, 25], we introduce a commensurate AFM order parameter:

$$\Delta = \frac{V}{\mathcal{V}} \sum_{\mathbf{k}} \langle a_{\mathbf{k}\sigma}^\dagger b_{\mathbf{k}+\mathbf{Q}_0-\sigma} \rangle \tag{5}$$

and diagonalize Hamiltonian (1). Following the procedure described in detail in Refs. [15] and [24], we derive an expression for the grand thermodynamic potential per unit volume:

$$\Omega = 4N_F \left\{ \frac{\Delta^2}{2} \left(\ln \frac{\Delta}{\Delta_0} - \frac{1}{2} \right) + T \int_0^\infty d\xi \ln [f_F(-\mu - \eta) f_F(\mu - \eta)] \right\}. \tag{6}$$

Here, T is the temperature, $f_F(\epsilon) = 1/[1 + \exp(\epsilon/T)]$ is the Fermi function, $\eta = \sqrt{\Delta^2 + \xi^2}$, and $\Delta_0 = \Delta(T=0, \mu=0)$ is the BCS-like AFM gap, in which the considered weak-coupling limit is equal to $\Delta_0 = \epsilon_F \exp(-1/N_F V) \ll \epsilon_F$.

We neglect here a possible existence of the AFM orders with slowly rotating magnetization axis or so-called incommensurate SDW phases [15, 24, 25]. However, taking into account incommensurate SDW complicates the formulas drastically but does not change significantly the main results. Moreover, the difference in the free energies between the incommensurate SDW and PM phases is small and the incommensurate SDW phase is very sensitive to disorder [24]. In many cases, it could not be really observed.

The equilibrium value of the gap is determined by minimizing Ω . Thus, we derive from (6):

$$\ln \frac{\Delta_0}{\Delta} = \int_0^\infty d\xi \frac{f_F(\eta - \mu) + f_F(\eta + \mu)}{\eta}. \tag{7}$$

The number of electrons per unit cell n is the sum of their numbers n_m in magnetic and non-magnetic n_r bands. We define the shift of the electron number from the position of the perfect nesting as:

$$x = n(\mu) - n_0 = n_m(\mu) - n_m(0) + n_r(\mu) - n_r(0), \tag{8}$$

where the value $n_0 = n(\mu = 0)$ corresponds to the perfect nesting. Since in any realistic case $T, \mu \ll \epsilon_F$, we can represent n_r as $n_r(\mu) = n_r(0) + N_r \mu$. Following the procedure described in Refs. [15] and [24], we can derive the equation for x in the form:

$$\frac{x}{x_0} = \frac{r\mu}{\Delta_0} + \frac{1}{\Delta_0} \int_0^\infty d\xi [f_F(\eta - \mu) - f_F(\eta + \mu)], \tag{9}$$

where $x_0 = 4\Delta_0 N_F \mathcal{V}_e$, \mathcal{V}_e is the unit cell volume, and $r = N_r/2N_F$. Equations (7) and (9) form a closed system of equations to determine the functions $\Delta(x, T)$ and $\mu(x, T)$.

The applied pressure P affects all parameters of the material: $V, m_{a,b}, \epsilon_{\min}^\alpha, \epsilon_{\max}^\alpha$, etc. It is evident that the main effect on the electron structure of the studied system with nesting occurs due to the shift of the Fermi level closer or farther from the ideal nesting position. It can be shown that this shift occurs mainly due to the change in the energy positions of the bands relative to each other. Without the loss of generality, we can assume that the pressure shifts only the position of the reservoir band, while magnetic bands remain untouched. The possible shifts of the magnetic bands in energy can be absorbed in the renormalization of the chemical potential. The change of other model parameters with P is less important, and can be neglected in the first approximation, if the pressure is not extremely high. There is some analogy with the electron–electron correlations. A weak electron–hole interaction is of importance since it opens a gap at the Fermi level, while weak electron–electron and hole–hole correlations give rise only to small corrections to this result, and they can be neglected.

The pressure shifts the position of the bottom of reservoir band by $\delta\epsilon$. A corresponding shift of the chemical potential under pressure is $\mu(P) - \mu(0)$, while the total number of electrons per unit cell n (and, consequently, x) does not change. The variation in the number of non-magnetic electrons (per unit cell) is:

$$\delta n_r = 2N_r \mathcal{V}_e [\mu(P) - \mu(0) - \delta\epsilon], \tag{10}$$

while the variation in the number of magnetic electrons is:

$$\delta n_m = 4N_m \mathcal{V}_e \int_0^\infty d\xi \{f[\eta - \mu(P)] - f[\eta + \mu(P)]\} - 4N_m \mathcal{V}_e \int_0^\infty d\xi \{f[\eta - \mu(0)] - f[\eta + \mu(0)]\}. \tag{11}$$

Let the system be perfectly nested if $P = P_n$, that is, $\mu(P_n) = 0$ and $x = 0$. For parameter $\delta\epsilon$, we assume its linear dependence on the pressure:

$$\delta\epsilon(P) = \frac{\partial \epsilon_{\min}^c}{\partial P} (P - P_n). \tag{12}$$

Substituting (10)–(12) into (9) with the replacement $\mu + \delta\mu \rightarrow \mu$ and taking into account the condition $x(P) = const = 0$, one obtains:

$$r\mu = \frac{r\mu}{\Delta_0} + \frac{1}{\Delta_0} \int_0^\infty d\xi [f_F(\eta - \mu) - f_F(\eta + \mu)], \tag{13}$$

where we introduce the dimensionless variable:

$$p = \frac{\partial \epsilon_{\min}^c}{\partial P} \frac{P - P_n}{\Delta_0}. \tag{14}$$

For fixed $x = 0$, (7) and (13) form a closed system of equations determining the functions $\Delta(p, T)$ and $\mu(p, T)$.

For $x \neq 0$, we simply have to replace $rp \rightarrow rp + x/x_0$ in the left-hand side of (13), taking into account that under doping, pressure $P = P_n$ corresponds to a perfect nesting.

Comparing (13) with (9), we see that in our model, the pressure acts effectively as a doping. The only difference is that the levels of this “effective doping” is proportional to r , that is, to the density of states of the reservoir electrons. When the reservoir is absent, the pressure changes nothing. This is an artifact of our approximation, where we (i) neglect the dependence of other model parameters on pressure, and (ii) (which is more important) neglect a possible change of the shapes of the Fermi surfaces of the magnetic bands. Indeed, when we fix the Fermi surfaces of the bands a and b to be spheres, the only possible way to destroy the ideal nesting is to change the relative radii (that is, the difference of the Fermi momenta $k_{Fa} - k_{Fb}$) of these spheres under pressure, which is prohibited due to the charge conservation law. When the reservoir is present, the imbalance in the magnetic electrons appears due to the unequal k_{Fa} and k_{Fb} can be compensated by the reservoir electrons. The possible effects related to the shape of the Fermi surface are discussed in Section 5.

We choose here the simplest possible linear pressure dependence of $\delta\epsilon(P)$ to avoid any unnecessary speculations. Note also that such a choice is reasonable since $\delta\mu(P) \ll \epsilon_F$ in any case. The sign of the derivative $\partial\epsilon_{\min}^c/\partial P$ depends on the specific properties of the system. However, the change in the sign of this parameter means only the change in the sign of the “effective doping” and does not affect the electronic properties of the system. For definiteness, below we assume that $\partial\epsilon_{\min}^c/\partial P > 0$.

We solve the system of (7) and (13) numerically to find the functions $\Delta(p, T)$ and $\mu(p, T)$. Using these results, we calculate the grand potential Ω and the free energy $F = \Omega + \mu n$, and construct the phase diagram of the model in the p – T plane. Below, we also use the dimensionless free energy defined as $f = F/(\Delta_0 x_0)$.

The dependence of the gap Δ on the pressure is similar to the dependence of the gap versus doping derived in Refs. [15] and [24]. The gap decreases with $P - P_n$ and vanishes to zero at some value of the applied pressure.

The calculated phase diagrams of the model in the (P, T) plane are shown in Fig. 1 for different values of the relative number of non-magnetic electrons. In these diagrams, we observe a significant temperature reentrance of the ordered phase at high pressure, which is an analog to that observed in the phase diagrams in the temperature-doping plane, where the reentrance disappears if we take into account the existence of the incommensurate SDW [15, 24]. However, here we postulate the ground state of the system to be homogeneous, which, in general, is not true, as it is shown, e.g., in Refs. [24] and [25], and is also demonstrated in the next section.

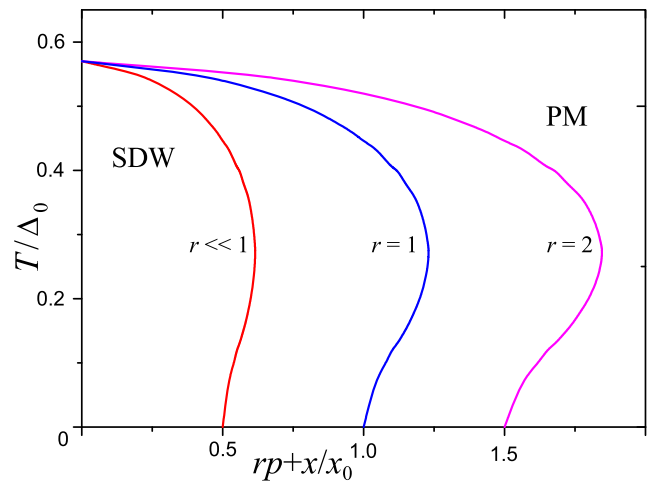


Fig. 1 (Color online) Phase diagram of the model in the (P, T) plane for different values of r : $r \ll 1$ – red line, $r = 1$ – blue line, and $r = 2$ – magenta line. A possibility of the existence of inhomogeneous phases is ignored. In the horizontal axis, we use effective doping (16), which is a linear function of P

3 Phase Separation: General Consideration

To consider the phase separation (PS), we have to study the doped system. As was mentioned above, for the finite doping x (13) becomes:

$$\frac{x_{\text{eff}}(P)}{x_0} = \frac{r\mu}{\Delta_0} + \frac{1}{\Delta_0} \int_0^\infty d\xi [f_F(\eta - \mu) - f_F(\eta + \mu)], \quad (15)$$

where we introduce the effective doping:

$$x_{\text{eff}}(P) = x + rx_0p. \quad (16)$$

We calculate the chemical potential μ as a function of x_{eff} . A typical result of such calculations in the case of $T < T^*$ is shown in Fig. 2. We see that the $\mu(x_{\text{eff}})$ behaves non-monotonically indicating an instability of the homogeneous state toward the phase separation. The separated phases are the SDW phase with effective doping $x_{\text{eff}}^{(1)}$ and the PM phase with effective doping $x_{\text{eff}}^{(2)}$. The parameters $x_{\text{eff}}^{(1,2)}$ are found using the Maxwell construction as shown in Fig. 2: the horizontal line crosses the curve $\mu(x_{\text{eff}})$ in such a way that shaded areas S_1 and S_2 are equal to each other [31]. The values of $x_{\text{eff}}^{(1,2)}$ depend on the model parameters and temperature, but do not depend on pressure. At the same time, the electron density in the phase-separated phases, $x_{1,2}$, depend on pressure. From (16), we obtain $x_{1,2} = x_{\text{eff}}^{(1,2)} - rx_0p$. If the volume fraction of the PM phase is c , then, from the charge conservation law, we have:

$$(1 - c)x_1 + cx_2 = x. \quad (17)$$

Thus, within the $x_1 < x < x_2$ doping range, the system’s ground state is a mixture of SDW phase with the electron

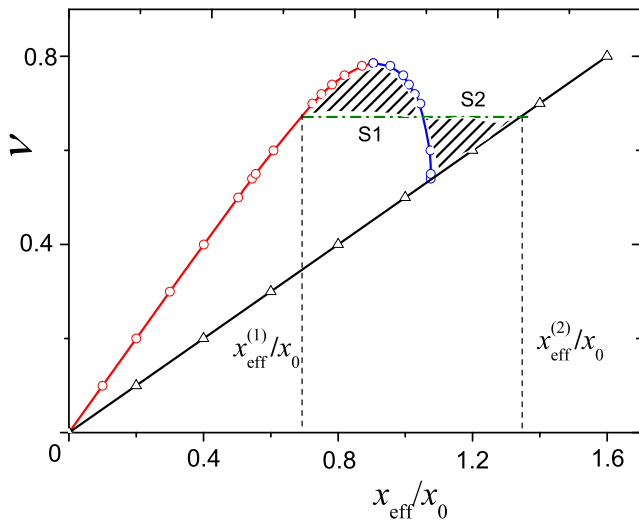


Fig. 2 (Color online) Dimensionless chemical potential $\nu = \mu/\Delta_0$ versus effective doping characterizing the shift of the electron density from the position of the perfect nesting. Here, we have $t = T/\Delta_0 = 0.1$ and $r = 1$. Ascending (red) and descending (blue) lines with circles correspond to the SDW phase, (black) line with up triangles – to the PM phase, and (green) dot-and-dash line shows the Maxwell construction with the areas $S_1 = S_2$

density $x_1 = x_{\text{eff}}^{(1)} - rx_0p$ and PM phase with the electron density $x_2 = x_{\text{eff}}^{(2)} - rx_0p$. This window shifts toward the smaller densities when the pressure increases. Let us consider the value of doping $x < x_{\text{eff}}^{(1)}$ (say, $x = 0$). At $P = P_n$ ($p = 0$), the ground state of the system is homogeneous SDW phase. Increasing p above the value $p_1 = (x_{\text{eff}}^{(1)} - x)/(rx_0)$ makes the system inhomogeneous. The fraction of the PM phase, c , gradually increases up to unity at $p = p_2 = (x_{\text{eff}}^{(2)} - x)/(rx_0)$. For $p > p_2$, the system is a homogeneous paramagnet.

As an illustration, the phase diagram of the model in the (P, T) plane is shown in Fig. 3 for $r \ll 1$ (a) and for $r = 2$ (b). The region of the possible inhomogeneous phase occupies a significant part of the phase diagram. The temperature reentrance in the phase diagram (see Fig. 1) disappears.

4 Phase Separation: the Structure of Inhomogeneous State

Determining the region of PS in Fig. 3, we neglected the contributions of the long-range Coulomb interaction arising due to the violation of the charge neutrality in the inhomogeneous phase, as well as the energy of the interface between SDW and PM phases. These terms not only affect the range of existence for the PS, but also determine the geometry of inhomogeneities [26, 27]. They depend on the volume fraction of the PM phase, c , the difference $x_1 - x_2$,

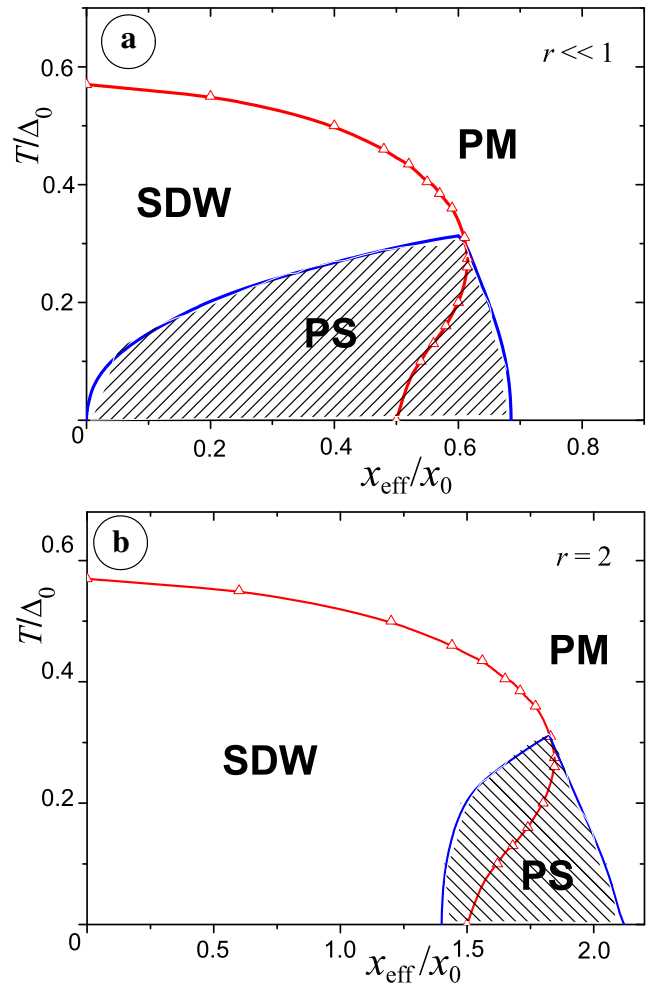


Fig. 3 (Color online) Phase diagram of the model in the (x_{eff}, T) plane in the cases $r \ll 1$ (a) and $r = 2$ (b). Solid (red) line with up triangles shows the boundary of the uniform stable SDW phase. The shaded area corresponds to the region with tendency to the phase separation (PS)

and on the characteristic size R_s and on the shape of the inhomogeneities. In general, we have to add such terms to the free energy, and if they are large, the phase separation is unfavorable [26, 27]. Moreover, when the electrostatic energy is comparable to the free energy gain due to the phase separation, both the “magnetic” and “nonmagnetic” charge carriers become redistributed and screen the local charge. However, further on, we will assume that the electrostatic and interface energies are small compared with the characteristic electron energy and we will use the values $x_{1,2}$ calculated in the previous section. The criterion of applicability of such approach will be presented below.

In our analysis, we follow Refs. [26] and [27]. In these papers, the three different geometries of inclusions were considered: droplets or islands (three-dimensional geometry, $D = 3$), rods or pillars ($D = 2$), and layers or slabs ($D = 1$). The minimization of sum E_{CS} of the

electrostatic and interface energies with respect to the size of inhomogeneities R_s gives [26, 27]

$$E_{CS} = 3 \left[\frac{e^2}{4\epsilon} (x_1 - x_2)^2 \sigma^2 c^2 D^2 u_D(c) \right]^{1/3}, \quad (18)$$

where ϵ is the average permittivity characterizing a polarization of the material due to the deviation from charge neutrality, σ is the interface tension, and $u_D(c)$ is a dimensionless function depending on the geometry of the inclusions. As a result, we have:

$$\begin{aligned} u_3(c) &= \frac{4\pi c}{5} (2 - 3c^{1/3} + c), \text{ droplets,} \\ u_2(c) &= \pi c (-\ln c + c - 1), \text{ rods,} \\ u_1(c) &= \frac{4\pi}{3} (1 - c)^2, \text{ layers.} \end{aligned} \quad (19)$$

Here, it is assumed that $c \leq 1/2$; otherwise, we must replace c in the above expressions by $1 - c$. In the framework of the same approximation, we can write the expression for the optimum R_s in the form [26, 27]:

$$R_s = \left[\frac{\sigma \epsilon}{2e^2 x_0^2} \cdot \frac{cD}{(x_1 - x_2)^2 u_D(c)} \right]^{1/3}, \quad (20)$$

where R_s is the droplet radius if $D = 3$, rod radius if $D = 2$, and slab half-width if $D = 1$.

For the inhomogeneous state, the dimensionless free energy $f = G/(\Delta_0 x_0)$ takes the form:

$$f_{PS} = (1 - c)f_F(x_1) + cf_F(x_2) + \lambda \varphi(c, x_1, x_2), \quad (21)$$

where $f(x_1)$ and $f(x_2)$ are the dimensionless free energies in the SDW and PM states with corresponding doping values, and:

$$\varphi = \left[cD(x_1 - x_2)\sqrt{u_D(c)} \right]^{2/3}, \quad \lambda = \frac{3}{\Delta_0 x_0} \left(\frac{ex_0\sigma}{4\sqrt{\epsilon}} \right)^{2/3}. \quad (22)$$

Note that, in general, it is difficult to estimate the value of λ , since we do not know the values of σ and the effective ϵ . To perform such calculations, it is necessary to consider a particular system.

It is evident that our approach is valid only in the case of $\lambda \ll 1$. Under the latter condition, we can apply the results obtained in the previous section. In this case, the electrostatic and interface energies do not affect significantly the range of existence for the phase separation but only determine the geometry of the inhomogeneous state. Namely [26, 27], the inclusions of the PM phase in the SDW host have the form of droplets ($D = 3$) if the PM phase content $c \lesssim 0.215$, rods or pillars ($D = 2$) if $0.215 \lesssim c \lesssim 0.355$, and slabs ($D = 1$) if $0.355 \lesssim c \lesssim 0.645$. At higher content of the PM phase, we have SDW rods in the PM host if $0.645 \lesssim c \lesssim 0.785$ and SDW droplets if $c \gtrsim 0.785$. However, if the content of the PM metallic phase is high, a percolative transition occurs in the sample from the low-conducting SDW-like behavior

to higher-conducting metal-like one. Then, in many cases, it is difficult to find out using the transport measurements, whether the PM metallic state is homogeneous or not.

As an illustration, the phase diagram of the system is shown in Fig. 4 in the case of $\lambda \ll 1$ and $x = 0$. The volume fraction of the PM phase, c , monotonically increases with pressure. As a result, the sequence of the geometries of inclusions changing with the growth of pressure will be the following: uniform SDW phase at low pressure is changed by PS with PM islands in the SDW host (area 1 in Fig. 4), then, by PM pillars (region 2), PM slabs (region 3), and, finally, there arise inclusions of the SDW phase in the PM host (regions 4 and 5). The latter inhomogeneous states could be seen as a uniform PM metallic state. The calculation procedure is the following. The content of the PM phase c can be expressed as (for $x = 0$):

$$c = \frac{rx_0p - x_{\text{eff}}^{(1)}}{x_{\text{eff}}^{(2)} - x_{\text{eff}}^{(1)}}, \quad (23)$$

where the values of the effective dopings $x_{\text{eff}}^{(1,2)}$ are calculated for a given temperature according to the Maxwell rule as described in the previous section.

5 Discussion

According to our speculations, the main effect of the pressure is due to the shift of the system from the nesting position. We assume that both electron and hole pockets

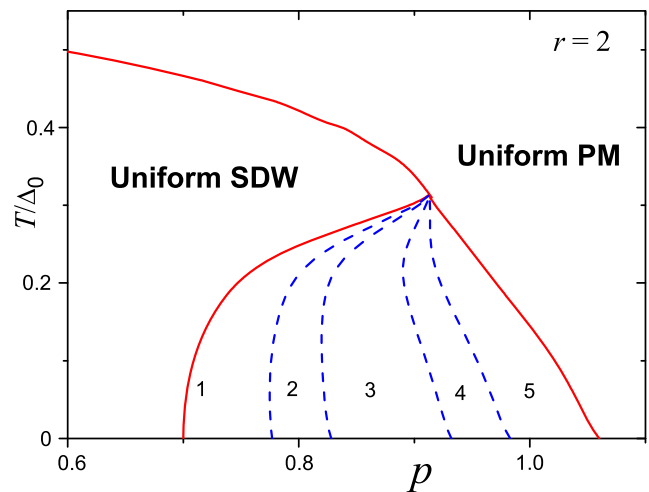


Fig. 4 (Color online) (P, T) phase diagram in the case $\lambda \ll 1$, $x = 0$, and $r = 2$. Solid (red) lines show the boundary of the uniform stable phases. Blue dashed lines show the boundaries of the inhomogeneous phases with different shapes of the inhomogeneities: PM droplets in the SDW host exist in region 1; PM pillars in the SDW host exist in region 2; alternating PM and SDW slabs exist in region 3; SDW pillars in the PM host exist in region 4; and SDW droplets in the PM host exist in region 5

have the shape of spheres. In this case, as it follows from (2) and (9), a shift of the electron system from the nesting position is characterized by the single parameter, namely, the dimensionless chemical potential:

$$\nu = \frac{\mu}{\Delta_0} \approx \frac{|k_{Fa} - k_{Fb}| \epsilon_F}{k_F \Delta_0} \quad (24)$$

When $\nu \ll 1$, the nesting is nearly perfect and $\Delta \approx \Delta_0$. With the increase of ν , the nesting becomes imperfect and the order parameter Δ considerably decreases if $\nu \approx 1$. When $\nu > 2 \div 3$, $\Delta = 0$, the SDW ordering and, consequently, the phase separation disappear. Since the ratio $\epsilon_F/\Delta_0 \gg 1$, the Fermi momenta of the electron and hole bands should be matched very closely to achieve a good nesting. The pressure destroys this matching giving rise to narrowing the range of SDW ordering and to the phase separation.

In our consideration, we assume that the pressure changes the values of k_{Fa} and k_{Fb} , but does not change the spherical geometry of the Fermi surface pockets. Naturally, it is a simplification. In particular, in superconducting iron pnictides, the electron and hole pockets have different shapes: the electron pockets are elliptical, while the hole ones are circular. The Bechgaard salts are highly anisotropic. We may expect that the Fermi surface of such salt is also anisotropic, and its nested parts are probably not spherical. In general, the pressure affects not only the value of the chemical potential, but also the geometry of the nested pockets. Thus, we need to include into consideration some additional geometrical factors, which governs the nesting. Note here that such an approach was applied for the analysis of the effect of doping in iron pnictides [21]. In this case, the de-nesting under pressure can occur even in the absence of the nonmagnetic reservoir. At the same time, if the electron and hole pockets are nested only partially, one can suggest that the SDW order parameter arises only in the nested parts of the Fermi surfaces, while other parts remain ungapped and play the role of the reservoir. Thus, one can expect that the model considered in this paper could be relevant, at least, qualitatively, even in the case of nonspherical Fermi surfaces. The detailed analysis of the effects of the Fermi surface geometry is a subject for future studies.

In fact, the de-nesting of any nature gives rise to the decrease of the SDW order and to the phase separation. With the increase of the pressure, the uniform SDW order transforms to the PS at some value of $P = P_0$. First, the inhomogeneous phase is a mixture of PM metallic droplets in the insulating SDW matrix. The volume concentration of the metallic phase increases with pressure and when $P = P_1$, the droplets merge to pillars and at $P = P_2 > P_1$ – to slabs, as it is shown in Fig. 4. With the further increase in pressure, $P > P_c$, the pillars and, then, droplets of the SDW phase exist in metallic matrix. However, the last

two inhomogeneous structures are frequently not revealed in the transport experiments since it is difficult to detect a small portion of insulating inclusions in the continuous metallic phase. We also may expect that the metallic phase is superconducting at low temperatures.

In Fig. 5a, we present the experimental results on the phase separation in the Bechgaard salt under pressure taken from Ref. [1]. In Fig. 5b, for comparison, we present a part of the phase diagram shown in Fig. 4 redrawn in the proper coordinates. We omit the inhomogeneous phases at high pressure assuming that at $P > P_c$, the sample is a metal from the experimental point of view. Qualitatively, the pictures illustrating the experimental and theoretical results are quite similar.

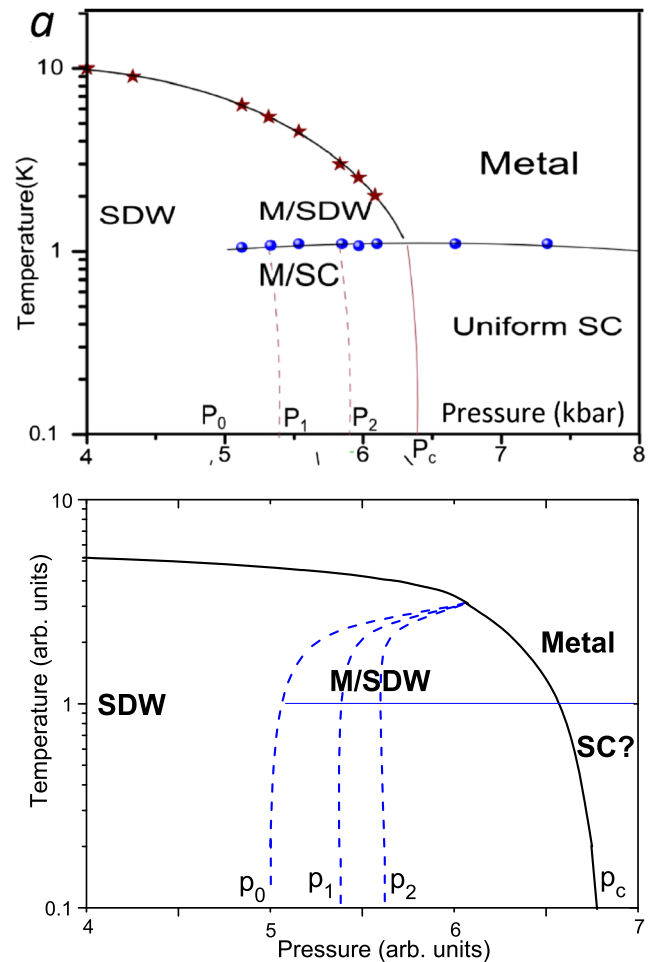


Fig. 5 (Color online) (a) Experimental observation of the PS in the Bechgaard salt [1] (Fig. 1 from Ref. [1]). The uniform SDW phase is observed if pressure $P < P_0$. The inhomogeneous mixture of the SDW and PM metallic phases exists if $P_0 < P < P_c$. The PS state includes metallic droplets in the SDW host if $P_0 < P < P_1$, the metallic pillars in the SDW matrix if $P_1 < P < P_2$, and the metallic slabs in the SDW host if $P_2 < P < P_c$. When $P > P_c$ the sample is in the metallic state. The metal is superconducting if $T < T_c$, the dependence $T_c(P)$ is shown by (blue) solid line with circles. (b) A part of the phase diagram shown in Fig. 4 redrawn in different coordinates, the notation corresponds to panel (a)

In conclusion, we have analyzed the effect of pressure on the electronic properties and the phase separation in the weakly correlated electron system with the imperfect nesting of the Fermi surface. The interaction of electrons in the nested pockets of the Fermi surface gives rise to the SDW ordering. The pressure shifts the electronic pockets from the nesting position resulting in a weakening of the SDW order and in the phase separation. The inhomogeneous phase is a mixture of the SDW insulator and PM metal. The geometry of the inhomogeneous phase depends on the volume content of the PM metal and, consequently, on the pressure. The obtained results allow us to understand the physical mechanisms underlying the experimental observation of the PS in Bechgaard salts [1]. They can also be a good addition to the usual analysis of the electronic phase separation [28–30].

Funding information This work is partially supported by the Russian Foundation for Basic Research (projects Nos. 17-02-00323, 17-02-447 00135, 19-52-50015, 19-02-00421, and 20-02-00015) and by the Presidium of Russian Academy of Sciences (program No. I.7).

References

- Narayanan, A., Kiswandhi, A., Graf, D., Brooks, J., Chaikin, P.: Coexistence of spin density waves and superconductivity in $(\text{TMTSF})_2\text{PF}_6$. *Phys. Rev. Lett.* **112**, 146402 (2014)
- Lee, I.J., Brown, S.E., Yu, W., Naughton, M.J., Chaikin, P.M.: Coexistence of superconductivity and antiferromagnetism probed by simultaneous nuclear magnetic resonance and electrical transport in $(\text{TMTSF})_2\text{PF}_6$ system. *Phys. Rev. Lett.* **94**, 197001 (2005)
- Vuletić, T., Auban-Senzier, P., Pasquier, C., Tomić, S., Jérôme, D., Hürtner, M., Bechgaard, K.: Coexistence of superconductivity and spin density wave orderings in the organic superconductor $(\text{TMTSF})_2\text{PF}_6$. *Eur. Phys. J. B* **25**, 319 (2002)
- Kang, N., Salameh, B., Auban-Senzier, P., Jérôme, D., Pasquier, C.R., Brazovskii, S.: Domain walls at the spin-density-wave endpoint of the organic superconductor $(\text{TMTSF})_2\text{PF}_6$ under pressure. *Phys. Rev. B* **81**, 100509 (2010)
- Agrestini, S., Saini, N.L., Bianconi, G., Bianconi, A.: The strain of CuOS_2 lattice: The second variable for the phase diagram of cuprate perovskites. *J. Phys. A: Math. Gen.* **36**, 9133 (2003)
- Makarov, I.A., Gavrichkov, V.A., Shneyder, E.I., Nekrasov, I.A., Slobodchikov, A.A., Ovchinnikov, S.G., Bianconi, A.: Effect of CuO_2 lattice strain on the electronic structure and properties of high- T_c cuprate family. *J. Supercond. Nov. Magn.* **32**, 1927 (2019)
- Sboychakov, A.O., Rakhmanov, A.L., Kugel, K.I.: Effect of electron–lattice interaction on the phase separation in strongly correlated electron systems with two types of charge carriers. *J. Phys.: Condens. Matter* **22**, 415601 (2010)
- Campi, G., Bianconi, A., Poccia, N., Bianconi, G., Barba, L., Arrighetti, G., Innocenti, D., Karpinski, J., Zhigadlo, N.D., Kazakov, S.M., Burghammer, M., Zimmermann, M.v., Sprung, M., Ricci, A.: Inhomogeneity of charge-density-wave order and quenched disorder in a high- T_c superconductor. *Nature* **525**, 359 (2015)
- Post, K.W., McLeod, A.S., Hepting, M., Bluschke, M., Wang, Y., Cristiani, G., Logvenov, G., Charnukha, A., Ni, G.X., Radhakrishnan, P., Minola, M., Pasupathy, A., Boris, A.V., Benckiser, E., Dahmen, K.A., Carlson, E.W., Keimer, B., Basov, D.N.: Coexisting first- and second-order electronic phase transitions in a correlated oxide. *Nat. Phys.* **14**, 1056 (2018)
- Li, J., Pellicciari, J., Mazzoli, C., Catalano, S., Simmons, F., Sadowski, J.T., Levitan, A., Gibert, M., Carlson, E., Triscone, J.-M., Wilkins, S., Comin, R.: Scale-invariant magnetic textures in the strongly correlated oxide NdNiO_3 . *Nature Comm.* **10**, 4568 (2019)
- Campi, G., Poccia, N., Joseph, B., Bianconi, A., Mishra, S., Lee, J., Roy, S., Nugroho, A.A., Buchholz, M., Braden, M., Trabant, C., Zozulya, A., Müller, L., Viehhaus, J., Schüßler-Langeheine, C., Sprung, M., Ricci, A.: Direct visualization of spatial inhomogeneity of spin stripes order in $\text{La}_{1.72}\text{Sr}_{0.28}\text{NiO}_4$. *Condens. Matter* **4**, 77 (2019)
- Kugel, K.I., Rakhmanov, A.L., Sboychakov, A.O., Poccia, N., Bianconi, A.: Model for phase separation controlled by doping and the internal chemical pressure in different cuprate superconductors. *Phys. Rev. B* **78**, 165124 (2008)
- Bianconi, A., Poccia, N., Sboychakov, A.O., Rakhmanov, A.L., Kugel, K.I.: Intrinsic arrested nanoscale phase separation near a topological Lifshitz transition in strongly correlated two-band metals. *Supercon. Sci. Tech.* **28**, 024005 (2015)
- Jaouen, T., Hildebrand, B., Mottas, M.-L., Di Giovannantonio, M., Ruffieux, P., Rumo, M., Nicholson, C.W., Razzoli, E., Barreateau, C., Ubaldini, A., Giannini, E., Vanini, F., Beck, H., Monney, C., Aebi, P.: Phase separation in the vicinity of Fermi surface hot spots. *Phys. Rev. B* **100**, 075152 (2019)
- Rice, T.M.: Band-structure effects in itinerant antiferromagnetism. *Phys. Rev. B* **2**, 3619 (1970)
- Fawcett, E.: Spin-density-wave antiferromagnetism in chromium. *Rep. Progr. Phys.* **60**, 209 (1988)
- Singh, D.J., Du, M.-H., Zhang, L., Subedi, A., An, J.: Electronic structure, magnetism and superconductivity of layered iron compounds. *Phys. C* **469**, 886 (2009)
- Vorontsov, A.B., Vavilov, M.G., Chubukov, A.V.: Superconductivity and spin-density waves in multiband metals. *Phys. Rev. B* **81**, 174538 (2010)
- Gor'kov, L.P., Teitel'baum, G.B.: Spatial inhomogeneities in iron pnictide superconductors: The formation of charge stripes. *Phys. Rev. B* **82**, 020510(R) (2010)
- Dai, P., Hu, J., Dagotto, E.: Magnetism and its microscopic origin in iron-based high-temperature superconductors. *Nat. Phys.* **8**, 709 (2012)
- Sboychakov, A.O., Rozhkov, A.V., Kugel, K.I., Rakhmanov, A.L., Nori, F.: Electronic phase separation in iron pnictides. *Phys. Rev. B* **88**, 195142 (2013)
- Rakhmanov, A.L., Rozhkov, A.V., Sboychakov, A.O., Nori, F.: Instabilities of the AA-stacked graphene bilayer. *Phys. Rev. Lett.* **109**, 206801 (2012)
- Gor'kov, L.P., Mnatzakanov, T.T.: Role of anisotropy in exciton transitions. *Sov. Phys. JETP* **36**, 361 (1973)
- Rakhmanov, A.L., Rozhkov, A.V., Sboychakov, A.O., Nori, F.: Phase separation of antiferromagnetic ground states in systems with imperfect nesting. *Phys. Rev. B* **87**, 075128 (2013)
- Sboychakov, A.O., Rakhmanov, A.L., Kugel, K.I., Rozhkov, A.V., Nori, F.: Magnetic field effects in electron systems with imperfect nesting. *Phys. Rev. B* **95**, 014203 (2017)
- Lorenzana, J., Castellani, C., Di Castro, C.: Phase separation frustrated by the long-range Coulomb interaction. I. Theory. *Phys. Rev. B* **64**, 235127 (2001)
- Kugel, K.I., Rakhmanov, A.L., Sboychakov, A.O., Kusmartsev, F.V., Poccia, N., Bianconi, A.: A two-band model for the phase separation induced by chemical mismatch pressure in different

- cuprate superconductors. *Supercond. Sci. Technol.* **22**, 014007 (2009)
28. Dagotto, E.: *Nanoscale Phase Separation and Colossal Magnetoresistance: The physics of Manganites and Related Compounds*. Springer Science, Berlin (2003)
29. Nagaev, E.L.: *Colossal Magnetoresistance and Phase Separation in Magnetic Semiconductors*. World Scientific, Singapore (2002)
30. Kagan, M.Y.u., Kugel, K.I.: Inhomogeneous charge distributions and phase separation in manganites. *Phys. Usp.* **44**, 553 (2001)
31. Landau, L.D., Lifshitz, E.M.: *Statistical Physics pt. I*. Pergamon, Oxford (1980)

Publisher's Note Springer Nature remains neutral with regard to jurisdictional claims in published maps and institutional affiliations.